

## Article

# Research on NaCl-KCl High-Temperature Thermal Storage Composite Phase Change Material Based on Modified Blast Furnace Slag

Gai Zhang <sup>1,2</sup>, Hui Cui <sup>1</sup>, Xuecheng Hu <sup>1</sup>, Anchao Qu <sup>1</sup>, Hao Peng <sup>1,3,\*</sup> and Xiaotian Peng <sup>1,\*</sup> 

<sup>1</sup> School of Mechanical and Power Engineering, Nanjing Tech University, No. 30 Pu Zhu South Road, Nanjing 211816, China; zhanggai@njtech.edu.cn (G.Z.); 202361207150@njtech.edu.cn (H.C.); 202161207192@njtech.edu.cn (X.H.); 202061207156@njtech.edu.cn (A.Q.)

<sup>2</sup> China MCC22 Group Corporation Ltd., No. 16, Xingfu Road, Tangshan 063000, China

<sup>3</sup> Jiangsu Key Laboratory of Process Enhancement and New Energy Equipment Technology, No. 30 Pu Zhu South Road, Nanjing 211816, China

\* Correspondence: phsight1@hotmail.com (H.P.); pengxiaotian@njtech.edu.cn (X.P.); Tel.: +86-13914707690 (H.P.); +86-15651863063 (X.P.)

**Abstract:** The high-temperature composite phase change materials (HCPCMs) were prepared from solid waste blast furnace slag (BFS) and NaCl-KCl binary eutectic salt to achieve efficient and cost-effective utilization. To ensure good chemical compatibility with chlorine salt, modifier fly ash (FA) was incorporated and subjected to high-temperature treatment for the processing of industrial solid waste BFS, which possesses a complex chemical composition. The HCPCMs were synthesized through a three-step process involving static melting, solid waste modification, and mixing–cold pressing–sintering. Then, the influence of the modification method and the amount of SiC thermal conductivity reinforced material on chemical compatibility and thermodynamic performance was explored. The results demonstrate that the predominant phase of the modified solid waste is  $\text{Ca}_2\text{Al}_2\text{SiO}_7$ , which exhibits excellent chemical compatibility with chlorine salt. HCPCMs containing less than 50 wt.% chloride content exhibit good morphological stability without any cracks, with a melting temperature of 661.76 °C and an enthalpy value of 108.73 J/g. Even after undergoing 60 thermal cycles, they maintain good chemical compatibility, with leakage rates for melting and solidification enthalpies being only 6.3% and 0.23%, respectively. The equilibrium was achieved when 40 wt.% of chloride salt was encapsulated upon the addition of 10% of SiC, and the incorporation of SiC resulted in an enhancement of thermal conductivity for HCPCMs to 2.959 W/(m·K) at room temperature and 2.400 W/(m·K) at 200 °C, with an average increase of about 2 times. The cost of the prepared HCPCMs experienced a significant reduction of 81.3%, demonstrating favorable economic performance and promising prospects for application. The research findings presented in this article can offer significant insights into the efficient utilization of solid waste.

**Keywords:** phase change material; blast furnace slag; heat storage material; thermal energy storage; chloride salt



**Citation:** Zhang, G.; Cui, H.; Hu, X.; Qu, A.; Peng, H.; Peng, X. Research on NaCl-KCl High-Temperature Thermal Storage Composite Phase Change Material Based on Modified Blast Furnace Slag. *Energies* **2024**, *17*, 2430. <https://doi.org/10.3390/en17102430>

Academic Editor: Antonio Rosato

Received: 18 April 2024

Revised: 15 May 2024

Accepted: 17 May 2024

Published: 19 May 2024



**Copyright:** © 2024 by the authors. Licensee MDPI, Basel, Switzerland. This article is an open access article distributed under the terms and conditions of the Creative Commons Attribution (CC BY) license (<https://creativecommons.org/licenses/by/4.0/>).

## 1. Introduction

The development of renewable energy sources, such as solar energy, wind energy, tidal energy, etc. [1–3], is a crucial approach to substitute conventional fossil fuels like coal, oil, and natural gas [4,5]. However, it encounters challenges including unstable energy supply and limited usage scenarios [6]. The utilization of heat storage technology for converting energy into thermal form represents a dependable means to enhance the efficiency of energy utilization [7,8]. Currently, phase change thermal storage technology has been successfully implemented in various domains, encompassing solar thermal storage [9], industrial waste heat recovery [10,11], building energy conservation [12,13], batteries [14], and new-energy vehicles [15,16].

Inorganic salts, such as silicates, carbonates, nitrates, phosphates, and chloride salts, are widely employed as thermal storage materials due to their appropriate melting temperature, high heat storage capacity, and density [17,18]. However, the utilization of phase-change materials composed of inorganic salts is significantly restricted due to their unstable physical properties, lower thermal conductivity, and corrosiveness during the phase transition process [19,20]. The incorporation of high thermal conductivity and physically stable skeleton materials with inorganic salts for the preparation of composite phase change materials (CPCMs) can effectively enhance their durability and stability [21–23]. Common backbone materials for salt-based phase change materials (PCMs) include metallic materials [24,25], ceramic materials [21], and porous materials [23]. Zhang et al. [6] utilized kaolin as a backbone material to encapsulate a mixture of NaCl and KCl eutectic salts, utilizing direct mixing and sintering techniques to fabricate stable shape-stabilized phase-change materials (SSPCMs) suitable for high-temperature applications. The results demonstrate the favorable compatibility between kaolin and NaCl-KCl. With a salt content of 80 wt.% in the NaCl-KCl/kaolin clay composite material, the phase change enthalpy reaches 178 J/g while achieving an energy storage density of 171.32 J/cm<sup>3</sup>, indicating optimal performance. Li et al. [17] developed a ternary molten salt system consisting of LiNO<sub>3</sub>-NaNO<sub>3</sub>-NaCl and prepared CPCMs with expanded graphite (EG). Notably, the newly prepared nitrate–chloride mixed molten salt exhibited a lower phase transition temperature, a higher latent heat value, and a higher thermal decomposition temperature compared to LiNO<sub>3</sub>-NaNO<sub>3</sub> alone. Furthermore, when the EG content reached 20%, its thermal conductivity increased from 1.378 W/m·K to 5.453 W/m·K. Jiang et al. [26] utilized an innovative diatomite-based porous ceramic material in combination with NaNO<sub>3</sub> to fabricate shape-stable composite phase change materials (CPCMs). Additionally, a comprehensive analysis was conducted on the thermophysical properties of these CPCMs both prior to and following the modification of the framework materials of diatomite-based porous ceramics. The findings demonstrated that both types of framework materials effectively encapsulated NaNO<sub>3</sub>, thereby enhancing thermal stability and exhibiting excellent chemical compatibility with NaNO<sub>3</sub>.

The conventional mining and processing of skeleton materials inevitably lead to a significant release of carbon emissions, resulting in resource depletion and irreversible pollution in the surrounding environment [27]. Therefore, we have shifted our focus towards selecting industrial solid wastes as skeleton materials [28]. Blast furnace slag (BFS), an industrial by-product composed of silicates and chlorates generated during iron smelting, primarily consists of oxides such as CaO, SiO<sub>2</sub>, Al<sub>2</sub>O<sub>3</sub>, MgO, and a small amount of sulfide [29,30]. With an annual global production of approximately 390 million tons [31], most BFS is currently discarded or buried, causing severe harm to the natural environment and public health. The utilization of some portions for cement or concrete preparation is observed. However, the added value of BFS remains relatively limited [32].

Scholars have investigated the incorporation of BFS as a fundamental constituent in organic phase-change materials to develop innovative CPCMs. Zhang et al. [33] employed three common substances, namely, NaNO<sub>3</sub>, Al, and Na<sub>2</sub>SO<sub>4</sub>, for blending with BFS and subsequently prepared BFS-based CPCMs using the mixed-sintering technique. The findings indicated that Al and Na<sub>2</sub>SO<sub>4</sub> were unsuitable for forming composites with BFS. The thermophysical properties of CPCMs containing only 40 wt.% NaNO<sub>3</sub>/BFS were thoroughly characterized by their respective attributes. Qu et al. [34] further advanced CPCMs based on NaNO<sub>3</sub> and BFS while characterizing their properties concurrently. The outcomes demonstrated that the porous structure of pretreated BFS could effectively enhance the thermal stability of the encapsulated salt, leading to stable formation of 50 wt.% NaNO<sub>3</sub> within it. Moreover, these developed CPCMs exhibited exceptional thermophysical properties. However, it has been observed that NaNO<sub>3</sub> undergoes decomposition into noxious gases during high-temperature heat storage processes, and the phase transition temperature shall not exceed 350 °C, thereby restricting its practical application in the field.

To address the issue of low heat storage temperature and potential generation of harmful gases in the current slag-based composite inorganic salts, this paper takes NaCl-KCl binary eutectic salt as the phase-change material compounded with pretreated BFS to prepare CPCMs for high-temperature thermal storage, and uses FA as a modifier for modifying BFS. We characterize the modified CPCMs and study their chemical compatibility, microstructure, and thermodynamic properties. We then analyze the effect of different proportions of SiC nanoparticles on the heat transfer performance of CPCMs. Finally, we explore its potential application strategies and economic analysis.

## 2. Experimental Procedures

### 2.1. Experimental Materials

The details of the chemicals utilized in this paper are presented in Table 1.

**Table 1.** Selection and purchase of chemical reagent.

Materials	Fineness	Manufacturer
Coal ash	--	Maanshan Iron & Steel Company Limited, Ma'anshan, China
BFS	--	Maanshan Iron & Steel Company Limited, Ma'anshan, China
NaCl	AR, $\geq 99.5\%$	Shanghai McLean Biochemical Technology Co., Shanghai, China
KCl	AR, $\geq 99.5\%$	Shanghai McLean Biochemical Technology Co., Shanghai, China
Ultrafine silicon carbide powder	$\geq 99\%$ , 40 nm	Shanghai McLean Biochemical Technology Co., Shanghai, China

### 2.2. Experimental Instruments

The main parameters, including the primary experimental apparatus and models employed in this study, are presented in Table 2 below.

**Table 2.** Equipment required for the experiment.

Equipment Name	Model Number	Main Parameters	Manufacturer
Vacuum Drying Oven	DZF6020	Vacuum degree: $-0.1$ MPa	Shanghai Jiecheng Experimental Instrument Co., Shanghai, China
Electromagnetic crusher	DF-4	Temperature fluctuation: $\pm 0.1$ °C	Shaanxi (Yulin) Duger Electromechanical Equipment Co., Yulin, China
Electronic balance	BT125D	Feeding granularity $\leq 15$ mm	Sartoriussta, Germany
Tablet press	769YP-24B	Discharge particle size $\leq 3$ mm	Shanghai Xinnuo Instrument Co., Shanghai, China
Planetary ball mill	TM-400A	Range: 0–120 g	Beijing Aike Instrument and Equipment Technology Co., Beijing, China
High temperature chamber furnace	KSL-1700X-A3	Precision: 1/100,000	Hefei Kejing Material Technology Co., Hefei, China

### 2.3. Sample Preparation

The phase-change material NaCl-KCl was selected in this study, with FA used as a modifier to enhance the properties of BFS. The resulting modified BFS was used as the matrix material for preparing high-temperature stereotyped phase change heat storage materials derived from solid waste. The preparation process involved three main steps: eutectic salt preparation, solid waste modification, and mixing–cold pressing–sintering.

(1) Preparation of eutectic salt: Using the static melting method, NaCl and KCl were weighed out according to a specific ratio (NaCl:KCl molar ratio = 1:1.02). The salts were then dried at 80 °C for 1 h in a drying oven, followed by transfer into a planetary ball mill operating at a speed of 1000 r/min for 30 min. Subsequently, the thoroughly mixed salts were poured into a ceramic crucible and subjected to high-temperature phase change heat storage material synthesis using a box-sintering furnace. The sintering process was carried out in the box-type furnace with a heating rate of 5 °C/min until reaching 720 °C, which was maintained for 3 h. After completion of sintering, the crucible was cooled to

room temperature within the furnace before it was removed for sample collection. The collected sample was crushed using an electromagnetic crusher and further processed through planetary ball milling to obtain eutectic salt powder with the desired particle size.

(2) Solid waste modification: FA was employed as the modifier, while BFS was introduced into a ball mill (with a small amount of ball milling beads added). The ball milling speed was maintained at 150 r/min for 60 min, and the ball milling jar was opened every 20 min to tumble and stir the powder, preventing it from settling at the bottom. Subsequently, the mixed solid waste powder was compressed using a tablet press to obtain densified cylindrical solid waste blanks. These blanks were then placed in a sintering furnace and heated from room temperature to 1150 °C with a heating rate of 10 °C/min, followed by holding for 3 h. After the completion of sintering and cooling down of the furnace to room temperature, solid waste samples were extracted from crucibles and subsequently crushed using an electromagnetic crusher. Finally, solid waste powder with specific size requirements underwent planetary ball milling.

(3) Mixing–cold pressing–sintering process: The pre-treated solid waste powder and eutectic salt powder should be weighed in specific mass ratios, placed in a planetary mill with a small amount of grinding steel balls, and ground at 400 rpm for 30 min. After thorough mixing, approximately 1.0 g of pure water was added as an adhesive to each mixture before transferring them into a tablet press. We applied hydraulic compaction on the billet using a compression pressure of 10 MPa for one minute. Subsequently, the green billet with a diameter of 12.7 mm was placed in a vacuum drying oven at 105 °C for 12 h followed by sintering in an air atmosphere using a high-temperature box furnace. The temperature profile during the process was established as follows: initially, the temperature was elevated to 600 °C at a heating rate of 10 °C per minute and subsequently maintained for a duration of 10 min. Then, the temperature was further increased to 720 °C at a heating rate of 5 °C/min and maintained for 30 min. Subsequently, the temperature was gradually reduced to room temperature through natural cooling in order to obtain the final samples of high-capacity phase change materials (HCPCMs). The prepared HCPCMs were experimentally characterized to investigate their thermal storage properties.

### 3. Results and Discussion

#### 3.1. Analysis of Modified Solid Waste Materials

The BFS and FA used in this study were provided by Maanshan Iron and Steel Company (MISCO) and the chemical compositions of the two solid wastes are shown in Table 3. The LOI represents the loss on ignition.

**Table 3.** Chemical composition of BFS and FA.

BFS	Chemical composition	CaO	SiO <sub>2</sub>	Al <sub>2</sub> O <sub>3</sub>	MgO	SO <sub>3</sub>	Fe <sub>2</sub> O <sub>3</sub>	TiO <sub>2</sub>	K <sub>2</sub> O	LOI
		Content (wt.%)	43.73	27.36	15.42	7.24	2.24	1.04	1.02	0.72
FA	Chemical composition	SiO <sub>2</sub>	Al <sub>2</sub> O <sub>3</sub>	CaO	SO <sub>3</sub>	Fe <sub>2</sub> O <sub>3</sub>	TiO <sub>2</sub>	K <sub>2</sub> O	MgO	LOI
		Content (wt.%)	32.72	24.81	19.44	9.58	8.92	1.35	1.24	1.07

The two solid wastes BFS and FA were combined with NaCl-KCl binary eutectic salts to prepare BCPCMs based on BFS and FCPCMs based on FA. Then, the samples were subsequently sintered using a mixed sintering technique and subjected to X-ray diffraction (XRD) chemical compatibility experiments for analysis. The outcomes of these experiments are depicted in Figure 1. Upon comparing the diffraction peaks of the solid wastes, it is evident that these peaks disappeared from both BCPCM and FCPCM composites. Hence, effective modification of the two solid wastes becomes imperative in order to address their instability with eutectic chloride salt materials.

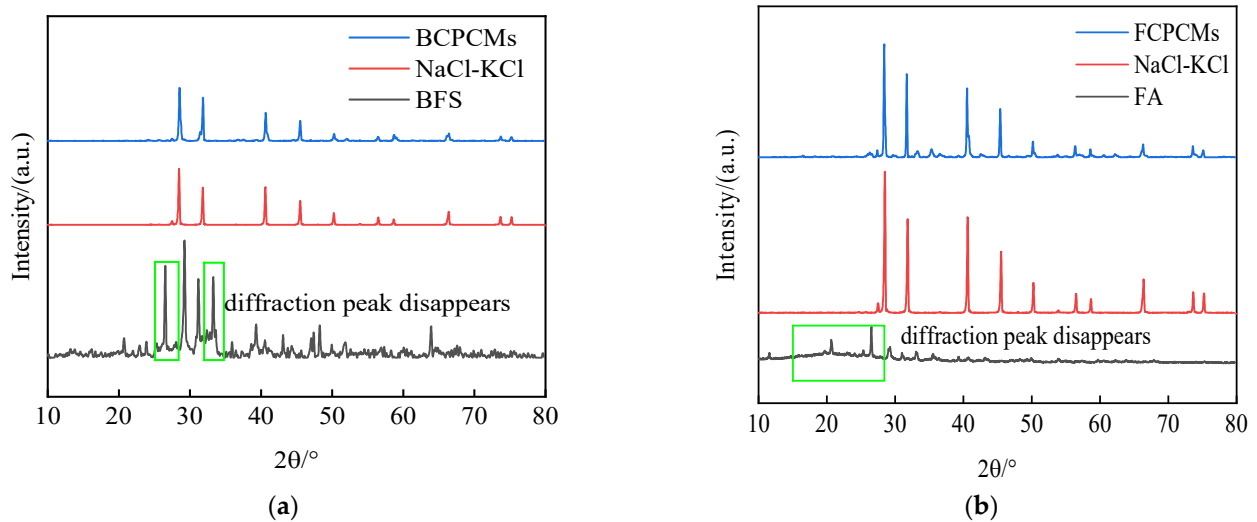


**Figure 1.** XRD patterns of slag, FA, and NaCl-KCl of Masteel Blast furnace and their composites. (a) BFS and NaCl-KCl chemical compatibility. (b) FA and NaCl-KCl chemical compatibility.

The solid waste modification method in this study is based on reference [35], which successfully achieved the production of stable calcium feldspar ceramic phase skeleton materials through high-temperature sintering of mixed solid wastes. Therefore, in this paper, BFS was utilized as the primary material to obtain stable calcium feldspar-like ceramic phase skeleton materials. FA was incorporated as a modifier and mixed with BFS at varying mass ratios. Subsequently, the compacted mixture of solid waste was subjected to high-temperature sintering and gradual cooling within a furnace environment. The XRD patterns illustrating the modified solid wastes obtained under different ratios and temperatures are presented in Figure 2.

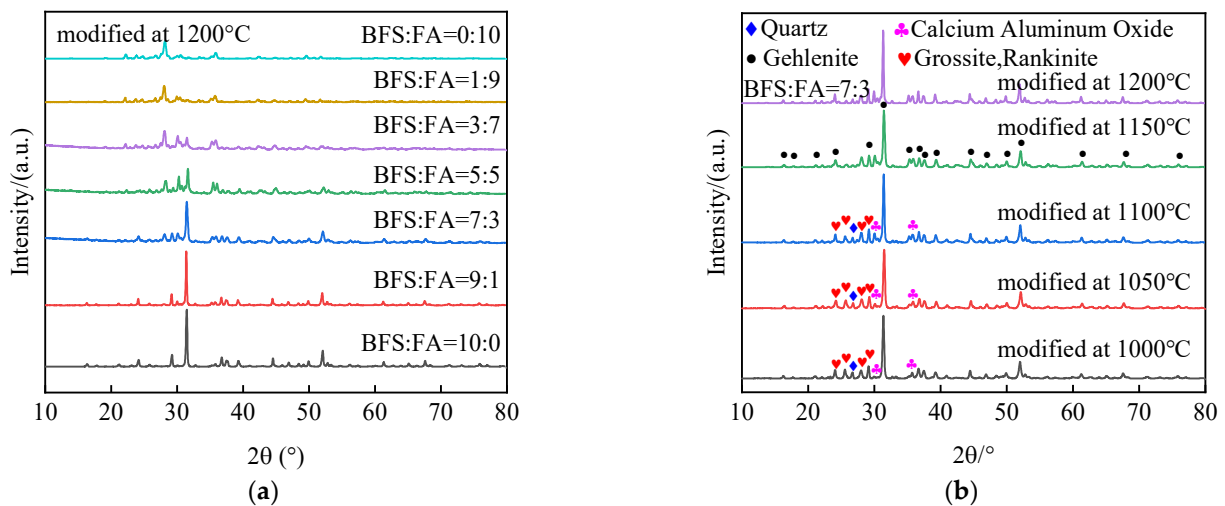


**Figure 2.** (a) Modified with different ratios. (b) Different modification temperatures.

In comparison, the phase composition of BFS is more distinct, primarily consisting of calcium–aluminum yellow feldspar (Gehlenite  $\text{Ca}_2\text{Al}_2\text{SiO}_7$ ), while the peaks corresponding to FA phases are comparatively lower than those observed for BFS, indicating a heterogeneous phase composition. The main phases in the mixed solid wastes were predominantly composed of substances with higher mass fractions under different ratios, except for BFS, FA, and mixed solid wastes at each ratio. After undergoing high-temperature treatment, the modified solid wastes exhibited stable diffraction peaks associated with their respective phases. However, a small number of impurity phases was also present. Based on these

findings, this paper presents an experimental study on temperature-based modification by incorporating 30 wt.% FA as a modifier and compounding it with 70 wt.% BFS.

To further investigate the influence of high-temperature environments on impurity phases in mixed solid waste, we conducted an XRD analysis of the modified solid waste, as shown in Figure 2b. The results indicate that the sintering temperature exceeds 1000 °C. The dominant phase structure observed in the modified solid waste is  $\text{Ca}_2\text{Al}_2\text{SiO}_7$ , with a minor presence of calcium aluminum oxide  $\text{CaAl}_2\text{O}_4$ , quartz (Quartz  $\text{SiO}_2$ ), and other mineral compositions at temperatures below 1150 °C. With increasing temperature, there is a gradual reduction in peak intensities for impurities such as quartz and other phases. In contrast, there is a significant enhancement in peak intensity for the calcium–aluminum pyritic feldspar phase, which remains relatively stable until reaching 1200 °C. Hence, it is inferred that the optimal sintering temperature for modifying mixed solid waste is approximately 1150 °C.

Through a comparative analysis of variations in quality, volume, and density between solid waste materials and modified solid waste before and after sintering, we guarantee compliance with stability requirements for the thermal storage system's practical implementation. This assessment employs the subsequent equations.

$$w_{\text{loss}} = \frac{w_{\text{end}} - w_{\text{beg}}}{w_{\text{beg}}} \times 100\% \quad (1)$$

$$V_{\text{exp}} = \frac{V_{\text{end}} - V_{\text{beg}}}{V_{\text{beg}}} \times 100\% \quad (2)$$

$$P_{\text{sh}} = \frac{P_{\text{end}} - P_{\text{beg}}}{P_{\text{beg}}} \times 100\% \quad (3)$$

The results are presented in Figure 3; the particles in the industrial solid waste blanks are either in point contact or separated from each other before sintering, resulting in a higher presence of pore structures. As temperature increases and time elapses, continuous internal material migration occurs within the solid waste billet, causing grain boundaries to shift and pore structures to be disrupted. This leads to contraction and subsequent exclusion of internal pores. Additionally, during the sintering process, a small amount of quality loss may occur due to particle adhesion on the crucible surface. Moreover, the main components  $\text{Al}_2\text{O}_3$  and  $\text{SiO}_2$  undergo a phase transition accompanied by slight volume expansion when forming mullite ( $\text{Al}_2\text{O}_3\text{-SiO}_2$ ) phase structure within the solid waste body, ultimately resulting in decreased density.

### 3.2. Chemical Compatibility

A comprehensive approach integrating theoretical and experimental methods was employed to investigate the chemical compatibility analysis of high-temperature stereotyped phase change thermal storage materials at elevated temperatures. The binary eutectic chloride salt (NaCl-KCl) primarily exists in the form of  $\text{Na}^+$ ,  $\text{K}^+$ , and  $\text{Cl}^-$  ions. Hence, it becomes imperative to conduct Gibbs free energy calculations for potential reactions between this eutectic chloride salt and industrial solid waste. Meanwhile, both sodium and potassium are classified as alkali metals in the first group of elements, and their ionic structures exhibit similarities. Consequently, the properties of their respective chlorides also demonstrate resemblances. Based on this premise, NaCl has been chosen as the subject of investigation to characterize high-temperature chemical reactions occurring in molten chloride salts within this paper. From a thermodynamic perspective, potential reactants with the binary eutectic salt include  $\text{Al}_2\text{O}_3$ ,  $\text{SiO}_2$ ,  $\text{CaO}$ ,  $\text{MgO}$ ,  $\text{MnO}$ ,  $\text{Fe}_2\text{O}_3$ ,  $\text{SO}_3$ , and  $\text{TiO}_2$ , among others. It is also worth noting that under elevated temperature sintering conditions, when combined with  $\text{SO}_3$  and  $\text{H}_2\text{O}$  molecules, NaCl may undergo decomposition.

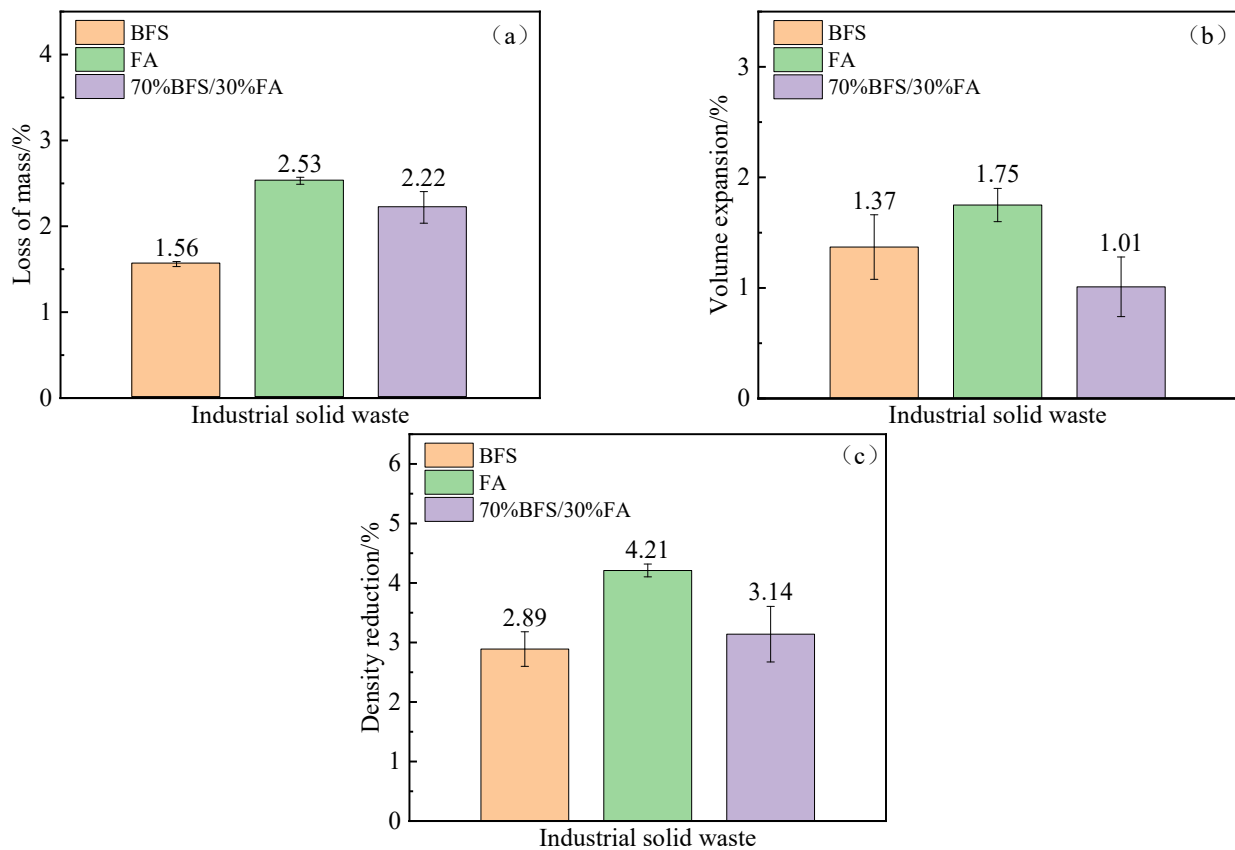
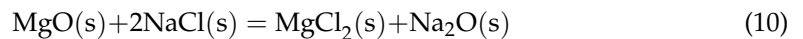
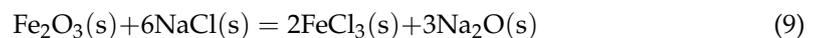
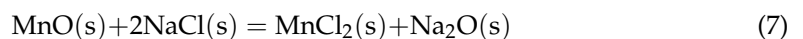
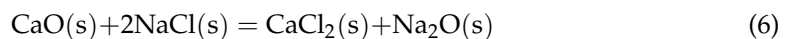
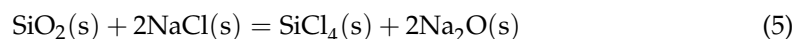
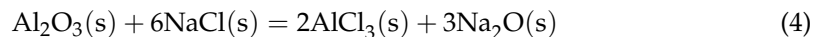


**Figure 3.** (a) Mass loss, (b) volume expansion, and (c) density reduction of solid waste after modification.

The potential chemical reactions are observed as follows:



The chemical thermodynamic data of pure substances were utilized to calculate the obtained data, which are presented in Figure 4 and Equations (4)~(10). In this study, the main metal oxide components in solid waste and NaCl-KCl eutectic salt are physically mixed without any chemical reaction occurring ( $\Delta_r G_m > 0$ ). The primary objective of solid waste modification is to enhance particle size and crystalline phase content, thereby achieving a stable physical composition with excellent thermal stability while avoiding significant chemical reactions. It should be noted that Equation (11) exhibits a reduced Gibbs free energy of 44.73 kJ/mol at 1300 K, gradually decreasing towards zero as temperature increases. This suggests that the application temperature for solid waste-based HCPCMs is more suitable below 1400 K. These results demonstrate the suitability of solid waste-based HCPCMs for practical applications.

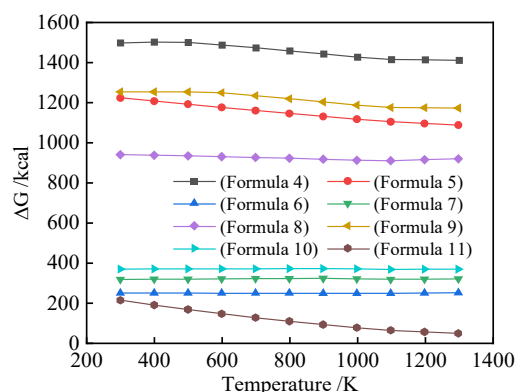


**Figure 4.** Gibbs free energy of modified solid waste components reacting with NaCl.

In order to validate the reliability of the aforementioned chemical reaction theory, this paper employs two experimental techniques, namely, XRD and Fourier transform infrared spectroscopy (FT-IR), for respective analysis. The XRD patterns of NaCl-KCl eutectic salt and its modified solid waste, as well as the hybrid composite phase change materials, are presented in Figures 5 and 6. The dominant peaks of NaCl-KCl are observed at  $2\theta = 31.692^\circ$ ,  $45.449^\circ$ ,  $28.345^\circ$ , and  $40.507^\circ$ , while those of the modified solid waste are located at  $2\theta = 29.131^\circ$ ,  $31.422^\circ$ , and  $52.094^\circ$ . The sintered HCPCMs only exhibit diffraction peaks corresponding to the modified solid waste and NaCl-KCl eutectic salt without any additional peaks. Meanwhile, Figure 7 illustrates the Fourier transform infrared spectra of NaCl-KCl eutectic salt, modified solid waste, and HCPCMs. The FTIR spectra of the modified solid wastes and HCPCMs exhibit consistent peak shapes characterized by two absorption bands spanning the range of  $400\text{--}4000\text{ cm}^{-1}$ . Notably, a prominent absorption band is observed between  $800\text{ and }1200\text{ cm}^{-1}$ , with a distinct peak at  $1066\text{ cm}^{-1}$  corresponding to the Si-O stretching vibration in  $\text{SiO}_4$  tetrahedrally connected to various oxygen atoms. Additionally, another absorption peak at  $920\text{ cm}^{-1}$  signifies the Si-O stretching vibration in  $\text{SiO}_4$  tetrahedrally bonded to different oxygen atoms. The absorption peak at  $920\text{ cm}^{-1}$  corresponds to the Si-O stretching vibration in the  $\text{SiO}_4$  tetrahedron, while the peak represents the bending vibrational absorption of Si-O-Al and Si-O-Si bonds. The sub-strong absorption band at  $400\text{--}600\text{ cm}^{-1}$  exhibits a peak at  $475\text{ cm}^{-1}$ , which is attributed to the bending vibration of Si-O. Conversely, no discernible peak shape was observed within the detection range for NaCl-KCl eutectic salt, resembling kaolinite behavior as reported by Zhang [6]. Therefore, it is inferred that modified solid waste and NaCl-KCl exhibit favorable chemical compatibility following high-temperature sintering.

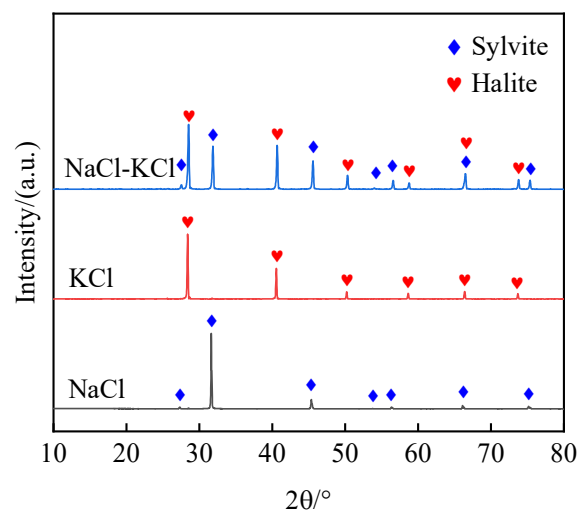


**Figure 5.** XRD pattern of NaCl-KCl eutectic salt.

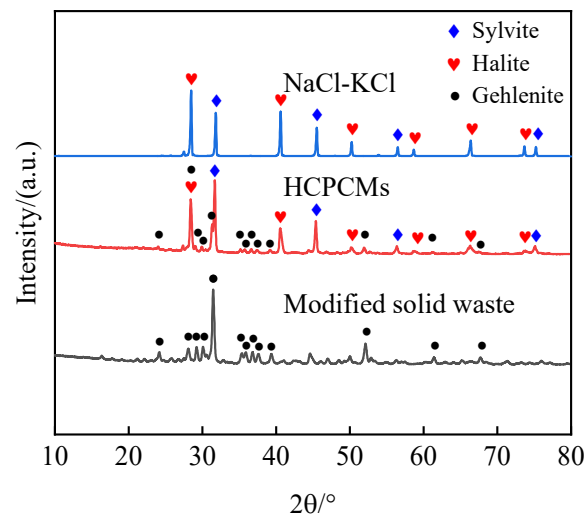


Figure 6. XRD pattern of NaCl-KCl eutectic salt.

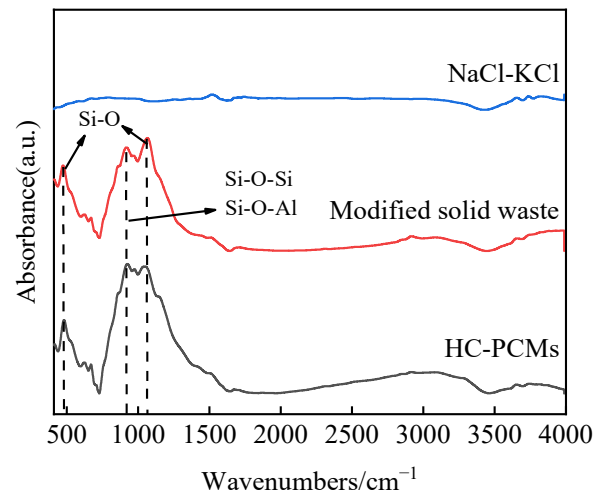


Figure 7. FT-IR pattern of NaCl-KCl eutectic salt, modified solid waste, HCPCMs.

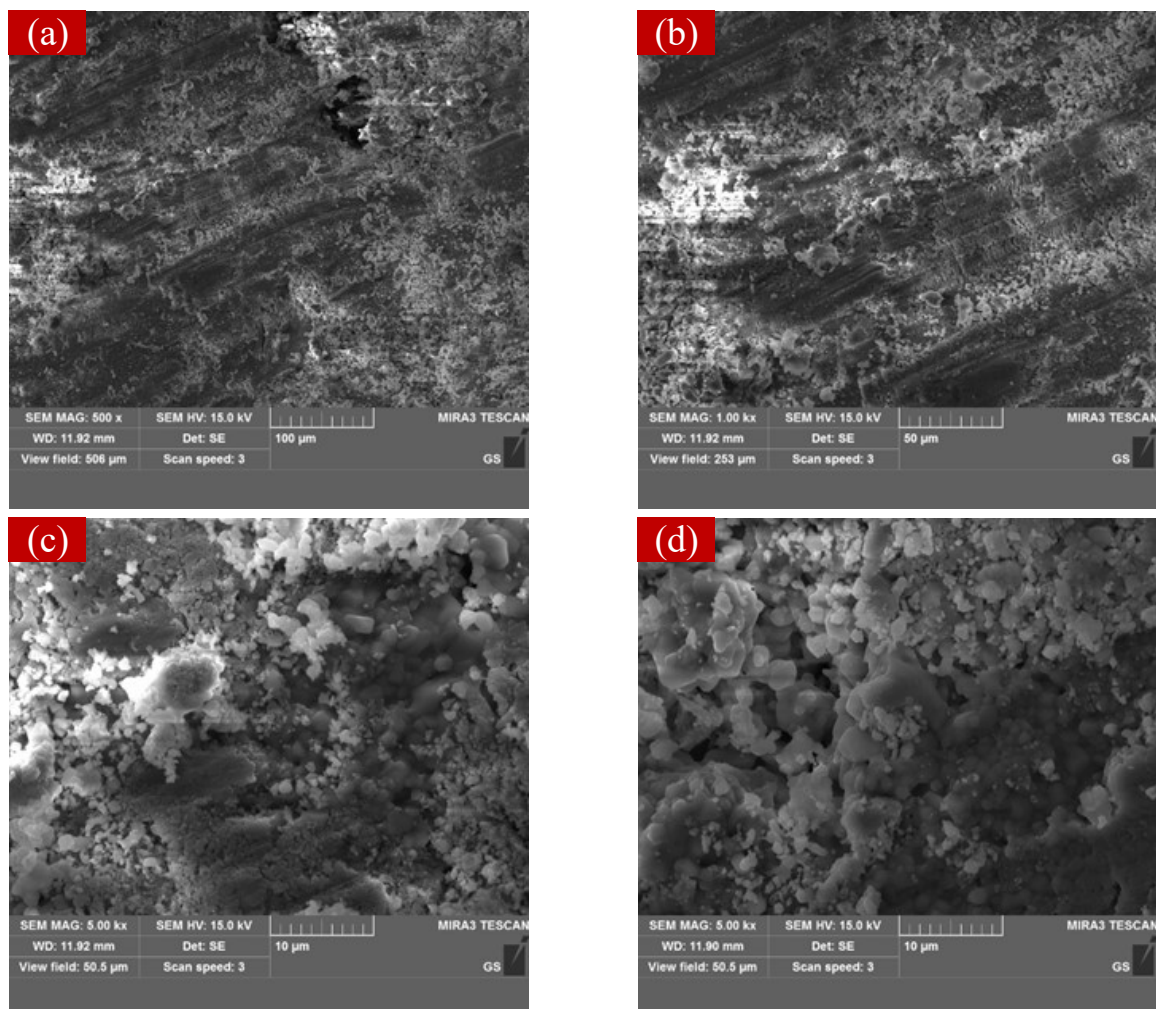
### 3.3. Morphological Features

The thermal storage units obtained by sintering with different ratios of inorganic salts and solid waste are presented in Figure 8. It is observed that HCPCMs exhibit significant expansion of their overall morphology after sintering at higher concentrations of NaCl-KCl due to the compactness of their internal structure, resulting in the leakage of inorganic salt PCMs. As shown in Figure 8, when modified solid wastes have a NaCl-KCl mass fraction exceeding 50%, expansion cracks are observed in the HCPCMs. This phenomenon is attributed to the contraction of the pore structure of the solid waste material during high-temperature modification, leading to some destruction of microporous structures and a reduction in overall porosity. Consequently, insufficient capillary force is generated during the encapsulation process to fully encapsulate excessive amounts of inorganic salt PCMs. When the NaCl-KCl content reaches 80 wt.%, complete collapse of HCPCMs occurs.

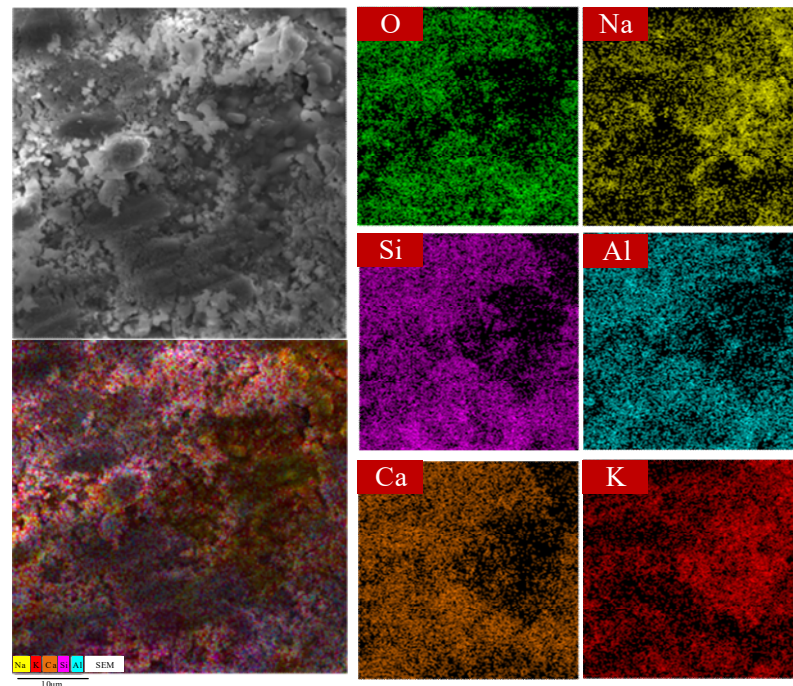


Figure 8. Macroscopic morphologies of solid waste matrix composites with different proportions.

The exceptional thermal storage performance of HCPCMs derived from solid waste primarily depends on the eutectic salt content within the coating. Therefore, significant attention has been devoted to investigating the unique pore structure exhibited by these waste materials. Figure 9 presents SEM microstructures of HCPCMs at different magnifications, revealing a composite material with a pore structure consisting of both large and small particles at the 10  $\mu\text{m}$  scale. Moreover, these porous structures contain embedded particles of various shapes and larger sizes. The elemental distributions obtained by the EDS surface scanning, as depicted in Figure 10, reveal that these particles are composed of a composite material known as NaCl-KCl eutectic salt PCMs. This observation also provides an explanation for the stable encapsulation of molten NaCl-KCl eutectic salt within the pore structure formed by modified solid waste particles at elevated temperatures in HCPCMs. Consequently, this structural arrangement effectively prevents PCM leakage and ensures robust support for maintaining the thermal energy storage capacity stability of HCPCMs. Furthermore, the microstructure diagram reveals the presence of unfilled microporous structures, which not only facilitate the flow and expansion of molten state phase change materials but also ensure overall morphological stability during exothermic charging processes.



**Figure 9.** SEM microstructure of HCPCMs at different magnifications (NaCl-KCl: BFS-FA, NaCl: KCl = 1:1.02, FA:BFS = 3:7) (a) 100  $\mu\text{m}$ , (b) 50  $\mu\text{m}$ , (c) 10  $\mu\text{m}$ , (d) 10  $\mu\text{m}$ .



**Figure 10.** SEM microstructure and element distribution of HCPCMs at 10  $\mu\text{m}$ .

### 3.4. Thermophysical Properties of HCPCMs

#### 3.4.1. Thermal Storage Properties

The potential application of thermal storage materials relies on their inherent thermal storage properties. Therefore, in this study, differential scanning calorimetry (DSC) experiments were conducted to analyze the latent heat behavior of HCPCMs containing varying mass fractions of inorganic salts. It is worth noting that the NaCl-KCl binary eutectic salt system with a molar ratio of 1:1.02 exhibits a melting point of 657  $^{\circ}\text{C}$ . Figure 11 illustrates the DSC curves obtained during the preparation process of NaCl-KCl eutectic salt with a molar ratio of 1:1.02 under heating conditions ranging from 500 to 700  $^{\circ}\text{C}$ . Notably, when the temperature reaches 656.44  $^{\circ}\text{C}$ , a distinct peak corresponding to the phase transition of the eutectic salt is observed, indicating an enthalpy range for solid–liquid transition at approximately 248.22 J/g.

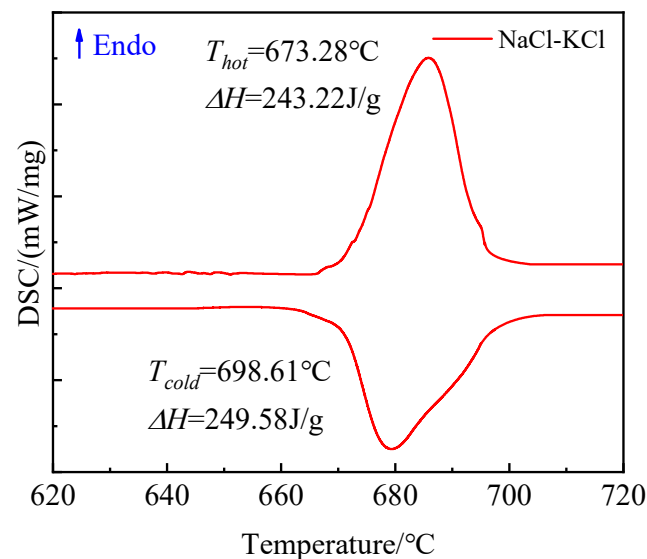


**Figure 11.** Latent heat DSC curve of pure NaCl-KCl eutectic salt.

Based on this, DSC experiments were conducted on three groups of HCPCMs with varying molar ratios of eutectic salts to modified solid wastes (3:7, 4:6, and 5:5) to investigate their thermal behavior in terms of appearance, morphology, and thermal storage properties. Measuring the enthalpy of molten eutectic chloride salt at high temperatures presents significant challenges due to its strong wetting behavior towards the alumina crucible, resulting in orderly creep along the crucible walls. Consequently, this leads to uneven temperature distribution within the vessel with thicker and thinner layers of eutectic chloride salt near and away from the wall, respectively, thereby impacting measurement accuracy. Therefore, each group of samples underwent three replicate measurements with identical masses during DSC analysis while conducting two cycles of melting/solidification. Subsequently, an average value was obtained for thermal analysis. The heat absorption/exothermic curves during the temperature change of HCPCMs, as illustrated in Figure 12, exhibited similarities to those of the eutectic salt NaCl-KCl. The onset temperatures of the heat absorption peaks corresponding to solid–liquid phase transition for the three groups of HCPCMs with molar ratios of 3:7, 4:6, and 5:5 were observed within the range of 659–652 °C. These values were slightly lower than that of pure eutectic salt with a melting temperature of 673.28 °C. Additionally, the respective latent heats of melting for these groups were measured at 64.73 J/g, 93.85 J/g, and 108.73 J/g.

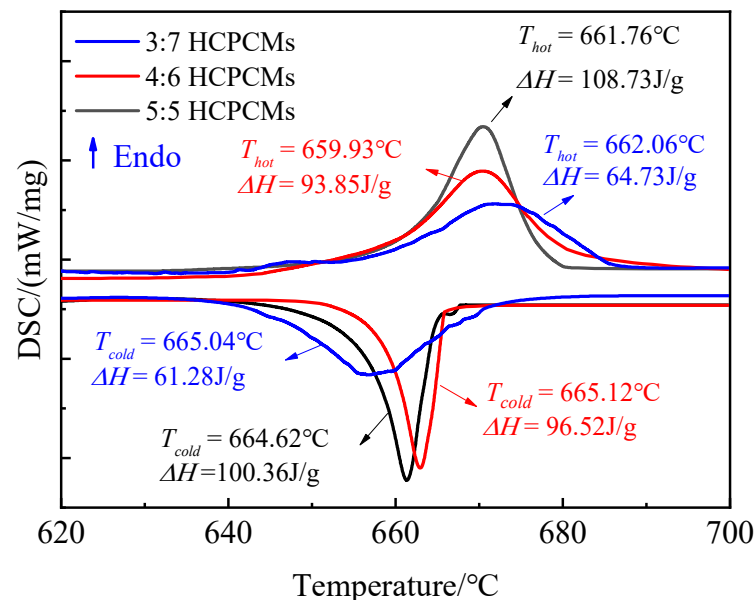


**Figure 12.** Latent heat DSC curves of shaped composites under different molar ratios.

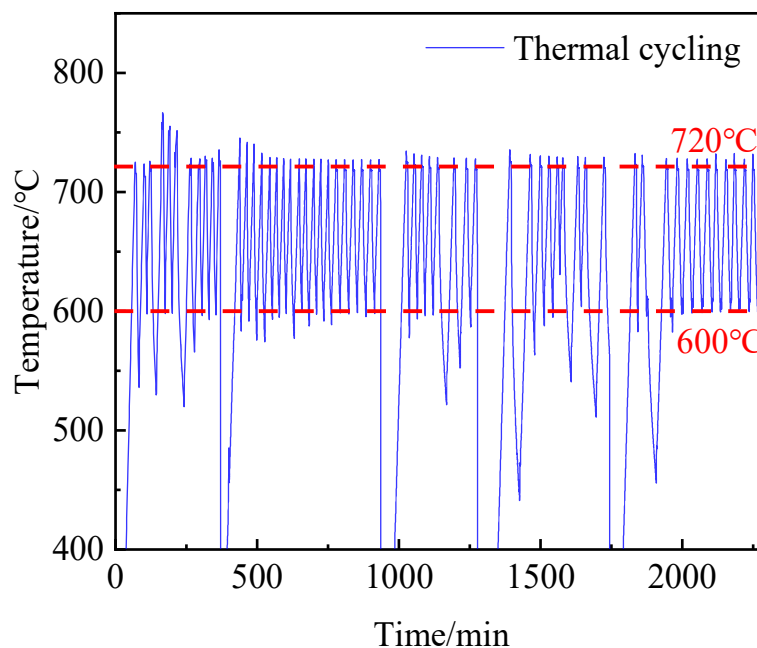
The theoretical values were calculated using the formula  $\Delta H_{\text{HCPCMs}} = \lambda \cdot \Delta H_{\text{pure}}$  and subsequently compared with the corresponding experimental values. The results presented in Table 4 demonstrate a slight disparity between the calculated theoretical latent heat values and the experimental measurements, with the latter exhibiting a minor deviation of less than 20% from the former. This observed phenomenon is attributed to the structural densification of the modified solid waste materials during the sintering process. Additionally, it is worth noting that the molten salts present on the side and bottom surfaces undergo a transition into a liquid state at elevated temperatures. However, due to their inherent mobility, these liquid molten salts are more susceptible to leakage from the skeleton material. The liquidity of the molten salt facilitates its extrusion from the skeleton material, and this microleakage increases proportionally with the content of PCMs. From the macroscopic morphology diagram, it is observed that when the PCM content exceeds 50 wt.%, there is a rapid escalation in leakage rate, thereby compromising both appearance stability and morphological integrity.

**Table 4.** Latent thermal properties of NaCl-KCl eutectic salt/modified solid waste composites at different ratios.

HCPCMs	Enthalpy of Melting $\Delta H$ (J/g)		Enthalpy of Solidification $\Delta H$ (J/g)	
	Experimental Value	Theoretical Value	Experimental Value	Theoretical Value
3:7	64.73	72.97	61.28	74.87
4:6	93.85	97.29	96.52	99.83
5:5	108.73	121.61	100.36	124.79
10:0	243.22	-	249.58	-

### 3.4.2. Thermal Cycling Stability

The composite materials undergo continuous thermal storage and exothermic processes during their practical application. Therefore, special attention should be paid to the thermophysical properties and thermal stability of HCPCMs after undergoing thermal cycling. To investigate this, composites containing 50 wt.% PCMs were subjected to 60 cycles of thermal cycling under experimental conditions. Figure 13 illustrates the temperature change curves during these cycles for HCPCMs, while the experimental samples were exposed to charging and exothermic cycling in sintering furnaces at temperatures ranging from 600 to 720 °C. The XRD analysis results presented in Figure 14 demonstrate that the samples exhibit consistent physical phases before and after cycling, without any evidence of new physical phases. This observation indicates exceptional thermal stability of HCPCMs. Additionally, Figure 15 depicts the storage and exothermic performance curves pre- and post-cycling. After undergoing 60 thermal cycles, a slight shift in the melting and solidification phase transition temperatures of HCPCMs was observed, accompanied by a decrease in the enthalpy of melting from 108.73 to 101.87 J/g. However, the enthalpy of solidification exhibited negligible change, with a leakage rate as low as merely 0.23%. This phenomenon is attributed to the volatilization and subsequent leakage of encapsulated PCMs during high-temperature sintering, leading to sample mass loss and alteration in enthalpy for phase transition.

**Figure 13.** Thermal cycling temperature variation of HCPCMs.

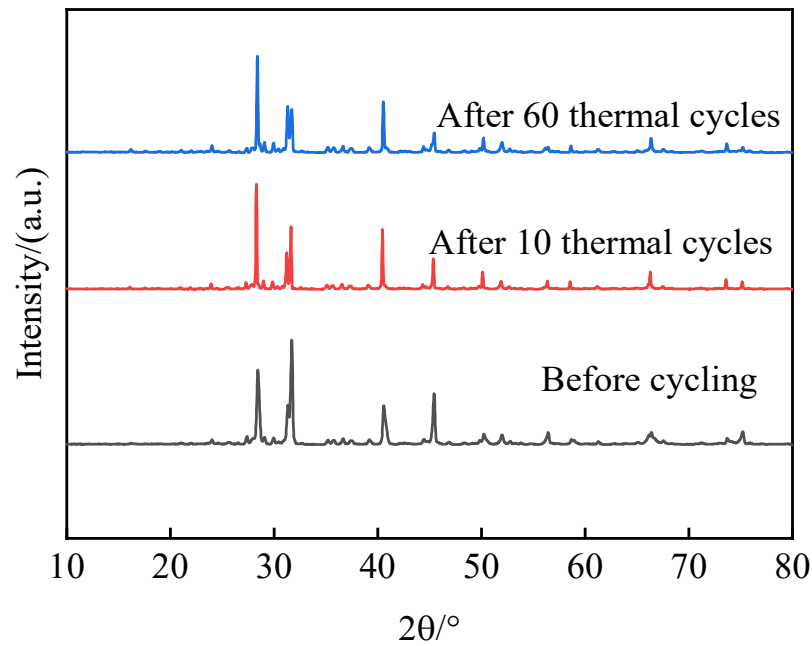


Figure 14. XRD patterns of HCPCMs before and after cycling.

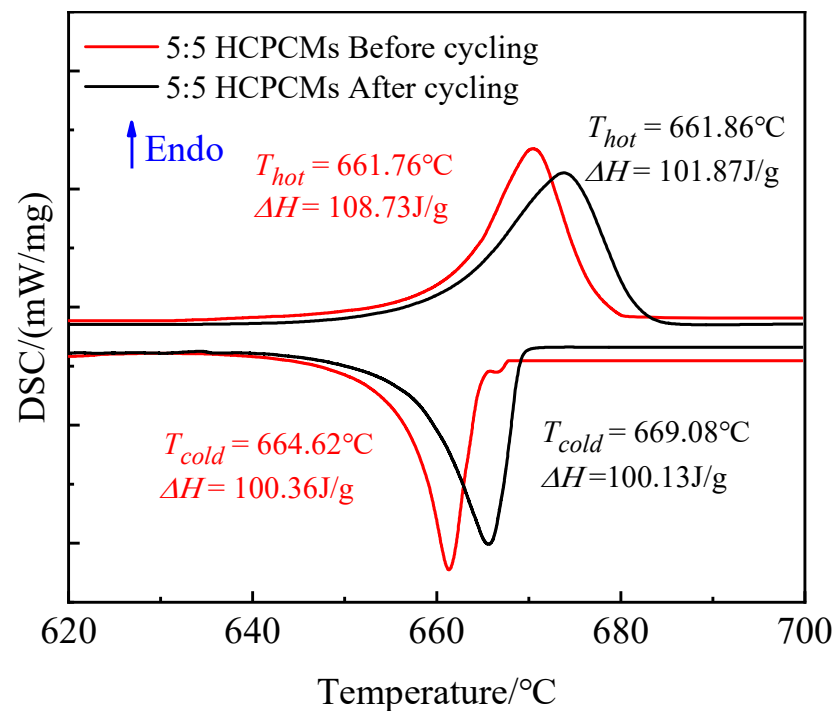
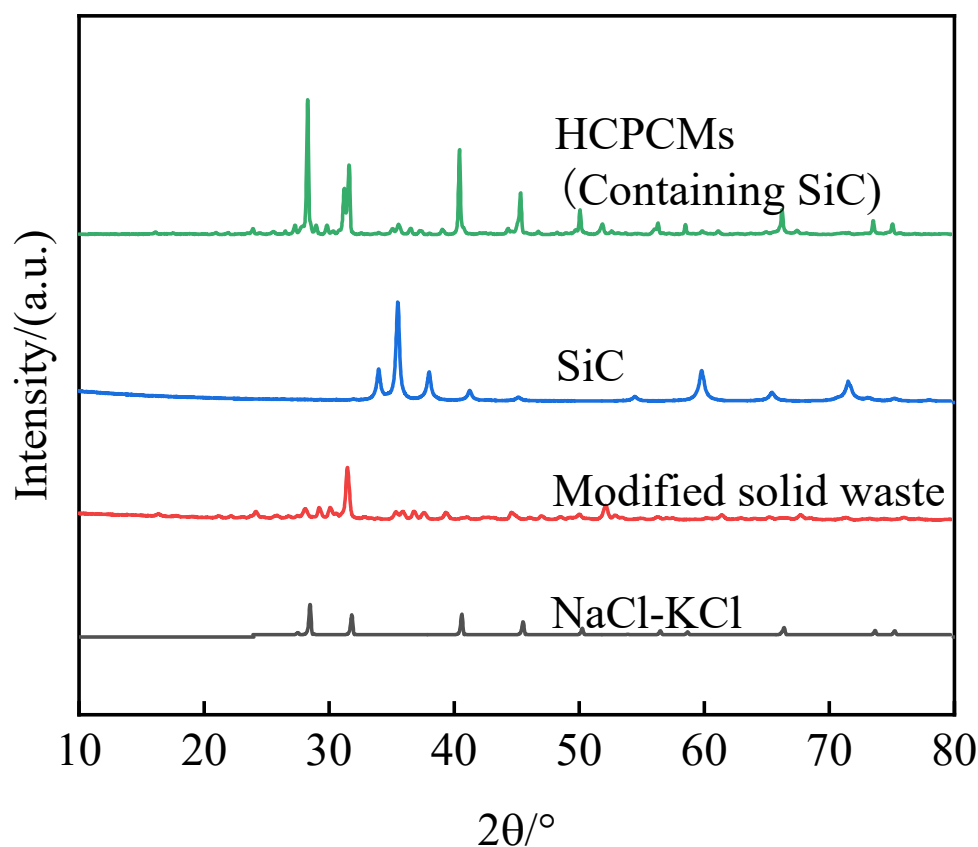


Figure 15. DSC curves before and after cycling of HCPCMs.

### 3.4.3. Thermal Conductivity Enhancement

The modification treatment of solid waste materials did not effectively enhance the thermal conductivity of HCPCMs. Consequently, ultrafine SiC particles with a thermal conductivity coefficient of approximately 300 W/(m·K) were incorporated as a thermal conductivity enhancement material, which were thoroughly dispersed within the internal structure of HCPCMs through mechanical ball milling and mixing processes to augment the heat transfer capability of the composite. The XRD patterns in Figure 16 illustrate the correspondence of diffraction peaks between SiC, NaCl-KCl, modified solid waste,

and thermally enhanced HCPCMs. Notably, there are variations in peak sizes while demonstrating a favorable chemical compatibility between SiC and the composite material.

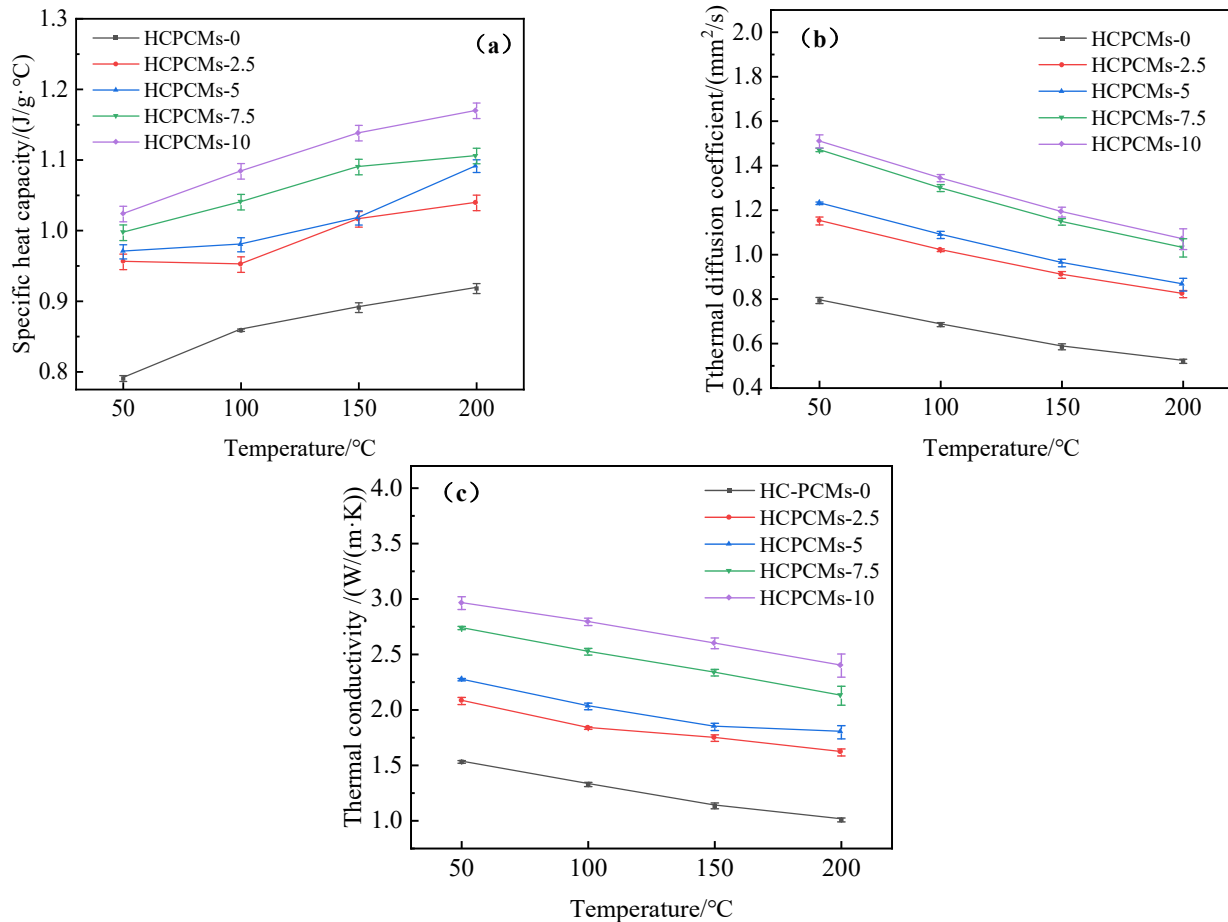


**Figure 16.** XRD patterns of HCPCMs, SiC, modified solid waste, and NaCl-KCl after enhanced thermal conductivity.

The HCPCMs with varying mass fractions of SiC are presented in Table 5, while the specific heat capacity, thermal diffusion coefficient, and thermal conductivity values of different HCPCMs at various temperatures are illustrated in the aforementioned graph (Figure 17). During temperature changes, the specific heat capacity values of different samples exhibit minimal variation and can be approximated as constant due to their representation of the substance's inherent ability to absorb heat, which is influenced by its type and state. Conversely, the thermal diffusion coefficient and thermal conductivity exhibit a gradual decline with increasing temperature. When HCPCMs are heated from 50 °C to 200 °C, the thermal conductivity experiences a reduction of approximately 0.5 W/(m·K). Moreover, the incorporation of SiC material significantly enhances both the thermal diffusion coefficient and thermal conductivity of HCPCMs. This enhancement is further augmented with an increase in SiC content. The initial thermal conductivity of HCPCMs-0 at 50 °C is merely 1.531 W/(m·K), whereas the addition of 10 wt.% SiC to HCPCMs elevates the thermal conductivity from 1.531 W/(m·K) to 2.959 W/(m·K), representing a remarkable increase of approximately 193%. As the temperature increases to 200 °C, there is a significant rise in the thermal conductivity of HCPCMs from 1.008 W/(m·K) to 2.4 W/(m·K), demonstrating an enhanced efficiency of approximately 238%. With increasing temperature and time, a continuous internal material migration occurred within the solid waste blanks, resulting in the degradation of the fine pore structure, contraction generation, and subsequent elimination of internal air voids. This densification process effectively mitigates contact thermal resistance, thereby enabling accurate prediction of the thermal conductivity of HCPCMs with SiC contents ranging from 2.5 wt.% to 10 wt.% through fitting a corresponding predictive equation based on experimental data.

**Table 5.** Content of each component in MCPCMs added with different contents of SiC.

HCPCMs	Mass Fraction of Each Component (wt.%)		
	NaCl-KCl	BFS/FA	SiC
HCPCMs-0	40	60	0
HCPCMs-2.5	40	57.5	2.5
HCPCMs-5	40	55	5
HCPCMs-7.5	40	52.5	7.5
HCPCMs-10	40	50	10

**Figure 17.** (a) Specific heat capacity, (b) thermal diffusion coefficient, and (c) thermal conductivity curves of HCPCMs with different SiC contents enhanced thermal conductivity.

### 3.5. Potential Applications

Due to the utilization of BFS as the underlying material, HCPCMs demonstrate exceptional physical stability in practical applications, eliminating the necessity for supplementary encapsulation containers. Consequently, HCPCMs can be fabricated into diverse geometries and integrated into customized modules suitable for a wide range of application scenarios.

The thermodynamic properties of the prepared HCPCMs investigated in this study offer two potential applications. Firstly, waste heat recovery is achieved by coupling waste heat with chemical reactions and production processes, resulting in a substantial release of thermal energy during industrial production. Therefore, these HCPCMs effectively serve thermal energy storage purposes when combined with a suitable heat absorption process aligned with the temperature range of the HCPCMs storing waste heat. Additionally, as the HCPCMs release heat during this coupling process, their temperature gradually

decreases, enabling them to be continuously coupled with an appropriate production process for the efficient release of stored heat. Moreover, HCPCMs can be utilized as a heat-insulating material by fabricating them into suitable modules and injecting them into the interlayer of high-temperature vessels based on practical application scenarios. These HCPCMs effectively absorb heat and mitigate temperature fluctuations within the vessel as the internal temperature increases. Simultaneously, these structures incorporate dedicated pathways for the circulation of cold fluid to facilitate efficient heat exchange with HCPCMs while ensuring equipment safety.

Based on the aforementioned applications, HCPCMs effectively serve as both heat transfer media and insulating materials, making them highly suitable for seamless integration into diverse renewable energy systems, facilitating efficient and safe low-carbon energy utilization. In practical thermal storage applications, further targeted research is needed on how to design the developed composite phase change material into a heat exchange device configuration with high thermal storage and release efficiency.

### 3.6. Economics Analysis

The economic analysis of HCPCMs is conducted through an estimation of the costs related to HCPCMs, followed by a comparison with their energy storage performance. The cost of C-PCM production primarily comprises the expenses associated with raw materials and manufacturing processes. The calculation method for material cost is to calculate the unit mass price of composite materials based on material proportion and unit price, as shown in Table 6.

**Table 6.** Relevant parameters in the material cost calculation (BFS-FA:NaCl-KCl:SiC = 5:4:1, BFS:FA = 7:3, NaCl:KCl = 1:1.02).

Constitute	BFS	FA	NaCl	KCl	SiC
Material expenses (\$/t) [36]	35	65	70	406	1700
Subtotal 1 (\$/t)			287.20		

The production cost encompasses the expenditure on energy, specifically electric power, involved in the preparation of HCPCMs. The cost of electricity is quantified by the amount of thermal energy absorbed during the preparation of HCPCMs. Consequently, the formula for calculating the production cost of HCPCMs is as follows [33]:

$$C_{produce} = \frac{Q_1}{Q_2 \times \eta} \times P \quad (12)$$

where represents the cost incurred during the production process (\$/t).  $Q_1$  denotes the energy density of HCPCMs in the production process (25–690 °C) measured in MJ/t.  $Q_2$  signifies the heat generated by natural gas during the production process of HCPCMs measured in MJ/t.  $\eta$  represents heating efficiency expressed as a percentage and  $P$  indicates the price of natural gas (USD/kW·h). The parameter values production cost calculation is presented in Table 7.

**Table 7.** Relevant parameters in the production cost calculation.

Constitute	$P$ (USD/m <sup>3</sup> )	$Q_1$ (MJ/t)	$Q_2$ (MJ/m <sup>3</sup> )	$\eta$ (%)
Production costs [37,38]	0.12	1104.36	36.00	30
Subtotal 2 (USD/t)			12.58	

The estimated cost of developing the new high-capacity phase change materials (HCPCMs) is USD 299.78/t, based on the provided information. Additionally, an analysis of their thermophysical properties reveals that the heat stored per ton of HCPCMs amounts

to only USD 2.76/MJ. According to a report published by the Department for Business, Energy, and Industrial Strategy (BEIS) in the UK, commercially operating conventional phase change materials (PCMs) should have a cost of less than EUR 50/kWh (USD 14.78/MJ). The current cost of these PCMs has decreased by 81.3% compared to the recommended threshold due to the utilization of cost-effective BFS and inorganic salts as raw materials. Consequently, the HCPCMs developed within this study demonstrate remarkable commercial competitiveness and exceptional thermophysical properties suitable for extensive large-scale applications.

#### 4. Conclusions

- Following modification by FA modifier and high-temperature treatment, the predominant physical phase of the modified BFS is calcium–aluminum yellow feldspar ( $\text{Ca}_2\text{Al}_2\text{SiO}_7$ ). This specific phase demonstrates excellent chemical compatibility with NaCl-KCl binary eutectic salts. Moreover, even after encapsulating chlorinated salts of PCMs up to 50 wt.%, the HCPCMs retain a stable morphology and structure.
- The melting temperatures of HCPCMs encapsulated with 30, 40, and 50 wt.% PCMs were approximately 661 °C, while the corresponding enthalpies measured closely approximated the theoretical values at 64.73 J/g, 93.85 J/g, and 108.73 J/g, respectively. Furthermore, exceptional thermal cycle stability was observed in terms of physical phase composition, microscopic morphology, and thermomechanical properties after 60 thermal cycles, with leakage rates for melting and solidification enthalpies being only 6.3% and 0.23%, respectively.
- The addition of 10 wt.% SiC demonstrates favorable morphological stability and significantly enhances the thermal conductivity of HCPCMs to 2.959 W/(m·K) at 50 °C, which is maintained at 2.400 W/(m·K) even at 200 °C, resulting in a remarkable two-fold enhancement across various temperature ranges with superior efficiency observed at elevated temperatures.
- The high-temperature composite phase change material prepared in this article has good application prospects in waste heat recovery and insulation materials, and the heat storage cost is about USD 2.95/MJ, which is decreased by 81.3% compared to the conventional heat storage cost. The research results of this article can provide important references for the efficient recycling and utilization of BFS and FA.

In the future, diverse modifiers can be further employed to enhance the modification of solid waste materials, optimize the phase composition of such materials, augment their porosity, accommodate a greater amount of inorganic salt PCMs, and enhance the energy storage density of composite materials.

**Author Contributions:** Conceptualization, G.Z. and X.P.; Methodology, G.Z. and H.C.; Software, G.Z. and X.H.; Validation, X.H. and H.C.; Formal analysis, G.Z. and A.Q.; Investigation, G.Z. and A.Q.; Resources, H.P. and X.P.; Data curation, G.Z. and X.H.; Writing, G.Z. and H.C.; Visualization, G.Z. and H.C.; Supervision, H.P. and X.P.; Project administration, H.P. and X.P.; Funding acquisition, X.P. All authors have read and agreed to the published version of the manuscript.

**Funding:** This study was supported by the Natural Science Foundation of the Jiangsu Higher Education Institutions of China (Grant NO. 23KJB470015), the Jiangsu Funding Program for Excellent Postdoctoral Talent (Grant No. 2023ZB756), and the Aeronautical Science Foundation of China (Grant No. 202300280T4002).

**Data Availability Statement:** Some or all data, models, or codes that support the findings of this study are available from the corresponding author upon reasonable request.

**Conflicts of Interest:** The authors declare that they have no known competing financial interests or personal relationships that could have appeared to influence the work reported in this paper.

## References

1. Guchhait, R.; Sarkar, B. Increasing Growth of Renewable Energy: A State of Art. *J. Energies* **2023**, *16*, 2665. [\[CrossRef\]](#)
2. Shi, S.; Liu, R.; Sheng, N.; Zhu, C.Y.; Rao, Z.H. Shape stabilized Al-Si/Al<sub>2</sub>O<sub>3</sub> phase change composites for high temperature heat storage. *J. Energy Storage* **2023**, *58*, 106425. [\[CrossRef\]](#)
3. Li, N.; Wang, Y.; Liu, Q.; Peng, H. Evaluation of thermal-physical properties of novel multicomponent molten nitrate salts for heat transfer and storage. *J. Energies* **2022**, *15*, 6591. [\[CrossRef\]](#)
4. Wang, Q.; Guo, J.L.; Li, R.R.; Jiang, X.T. Exploring the role of nuclear energy in the energy transition: A comparative perspective of the effects of coal, oil, natural gas, renewable energy, and nuclear power on economic growth and carbon emissions. *J. Environ. Res.* **2023**, *221*, 115290. [\[CrossRef\]](#)
5. Moriarty, P.; Honnery, D. Energy efficiency or conservation for mitigating climate change. *J. Energies* **2019**, *12*, 3543. [\[CrossRef\]](#)
6. Zhang, T.Y.; Wang, T.Y.; Wang, K.C.; Xu, C.; Ye, F. Development and characterization of NaCl-KCl/Kaolin composites for thermal energy storage. *J. Sol. Energy* **2021**, *227*, 468–476. [\[CrossRef\]](#)
7. Radouane, N. A comprehensive review of composite phase change materials (CPCMs) for thermal management applications, including manufacturing processes, performance, and applications. *J. Energies* **2022**, *15*, 8271. [\[CrossRef\]](#)
8. Ghosh, D.; Ghose, J.; Datta, P.; Kumari, P.; Paul, S. Strategies for phase change material application in latent heat thermal energy storage enhancement: Status and prospect. *J. Energy Storage* **2022**, *53*, 105179. [\[CrossRef\]](#)
9. Wang, X.; Liu, D.L.; Gao, G.Y.; Li, J.Y.; Yang, Z.D.; Lin, R.Y. Thermal performance study of a solar-coupled phase changes thermal energy storage system for ORC power generation. *J. Energy Storage* **2024**, *78*, 110126. [\[CrossRef\]](#)
10. Schwarzmayr, P.; Birkelbach, F.; Walter, H.; Javernik, F.; Schwaiger, M.; Hofmann, R. Packed bed thermal energy storage for waste heat recovery in the iron and steel industry: A cold model study on powder hold-up and pressure drop. *J. Energy Storage* **2024**, *75*, 109735. [\[CrossRef\]](#)
11. Hariti, Y.; Hader, A.; Faraji, H.; Boughaleb, Y. Scaling law of permeability and porosity for fluid transport phenomena in porous PCM media. *J. Appl. Comput. Mech.* **2021**, *7*, 84–92.
12. Gencil, O.; Bayram, M.; Subasi, S.; Hekimoglu, G.; Sari, A.; Ustaoglu, A.; Marasli, M.; Ozbakkaloglu, T. Microencapsulated phase change material incorporated light transmitting gypsum composite for thermal energy saving in buildings. *J. Energy Storage* **2023**, *67*, 107457. [\[CrossRef\]](#)
13. Babaharra, O.; Choukairy, K.; Faraji, H.; Hamdaoui, S. Improved heating floor thermal performance by adding PCM microcapsules enhanced by single and hybrid nanoparticles. *Heat Transf.* **2023**, *52*, 3817–3838. [\[CrossRef\]](#)
14. Ma, Y.; Wei, R.R.; Zuo, H.Y.; Zuo, Q.S.; Chen, Y.; Wu, S.Y.; Yang, H. Development of hierarchical MOF-based composite phase change materials with enhanced latent heat storage for low-temperature battery thermal optimization. *J. Energy* **2023**, *283*, 129001. [\[CrossRef\]](#)
15. Xie, P.; Jin, L.; Qiao, G.; Lin, C.; Barreneche, C.; Ding, Y.L. Thermal energy storage for electric vehicles at low temperatures: Concepts, systems, devices and materials. *J. Renew. Sustain. Energy Rev.* **2022**, *160*, 112263. [\[CrossRef\]](#)
16. Zhironkin, S.; Cehlar, M. Green economy and sustainable development: The outlook. *J. Energies* **2022**, *15*, 1167. [\[CrossRef\]](#)
17. Li, Y.; Zhou, S.H.; Jiang, S.L.; Tan, W.W.; Zhu, Q.Z. Preparation and thermal properties of LiNO<sub>3</sub>-NaNO<sub>3</sub>-NaCl/EG composite heat storage material. *J. Sol. Energy* **2023**, *263*, 111926. [\[CrossRef\]](#)
18. Sun, M.Y.; Liu, T.; Sha, H.A.; Li, M.L.; Liu, T.Z.; Wang, X.L.; Chen, G.J.; Wang, J.D.; Jiang, D.Y. A review on thermal energy storage with eutectic phase change materials: Fundamentals and applications. *J. Energy Storage* **2023**, *68*, 107713. [\[CrossRef\]](#)
19. Tiwari, V.; Periaswamy, S. Compatibility of structural materials with AlSi12 alloys-based phase change material and increasing the corrosion resistance by ceramic coatings. *J. Energy Storage* **2023**, *72*, 108526. [\[CrossRef\]](#)
20. Muzhanje, A.T.; Hassan, M.A.; El-Moneim, A.A.; Hassan, H. Preparation and physical and thermal characterizations of enhanced phase change materials with nanoparticles for energy storage applications. *J. Mol. Liq.* **2023**, *390*, 122958. [\[CrossRef\]](#)
21. Chang, Y.W.; Yao, X.Y.; Chen, Y.Y.; Huang, L.; Zou, D.Q. Review on ceramic-based composite phase change materials: Preparation, characterization and application. *J. Compos. Part B Eng.* **2023**, *254*, 110584. [\[CrossRef\]](#)
22. Chang, Y.W.; Yao, X.Y.; Chen, Y.Y.; Huang, L.; Zou, D.Q. Experimental study on the melting performance of phase change materials embedded with different material skeletons. *J. Appl. Therm. Eng.* **2024**, *236*, 121873.
23. Yang, X.M.; Li, C.B.; Ma, Y.F.; Chi, H.; Hu, Z.J.; Xie, J.F. High thermal conductivity of porous graphite/paraffin composite phase change material with 3D porous graphite foam. *J. Chem. Eng. J.* **2023**, *473*, 145364. [\[CrossRef\]](#)
24. Aljafari, B.; Kalidasan, B.; Kareri, T.; Alqaed, S.; Bhutto, Y.A.; Pandey, A.K. Organic/carbon and organic/carbon-metal composite phase change material for thermoelectric generator: Experimental evaluation. *J. Energy Storage* **2024**, *78*, 110082. [\[CrossRef\]](#)
25. Hu, T.; Wu, Z.; Fang, Y.; Niu, J.; Yuan, W.; Li, L. A novel metal-organic framework aerogel based hydrated salt composite phase change material for enhanced solar thermal utilization. *J. Energy Storage* **2023**, *58*, 106354. [\[CrossRef\]](#)
26. Jiang, F.; Ge, Z.W.; Ling, X.; Cang, D.Q.; Zhang, L.L.; Ding, Y.L. Improved thermophysical properties of shape-stabilized NaNO<sub>3</sub> using a modified diatomite-based porous ceramic for solar thermal energy storage. *J. Renew. Energy* **2021**, *179*, 327–338. [\[CrossRef\]](#)
27. Xiong, Y.X.; Wang, H.X.; Ren, J.; Nevzat, A.; Xu, Q.; Nie, B.J.; Li, C.; Ding, Y.L. Carbide slag recycling to fabricate shape-stable phase change composites for thermal energy storage. *J. Energy Storage* **2023**, *60*, 106694. [\[CrossRef\]](#)
28. Ghani, S.A.A.; Shafiqah, M.N.N.; Abidin, S.Z. Synthesis and characterization of stearic acid/waste filler materials as composite phase change material in thermal energy storage application. *J. Mater. Today Proc.* **2023**, *363*. [\[CrossRef\]](#)

29. Memon, S.A.; Lo, T.Y.; Barbhuiya, S.A.; Xu, W.T. Development of form-stable composite phase change material by incorporation of dodecyl alcohol into ground granulated blast furnace slag. *J. Energy Build.* **2013**, *62*, 360–367. [[CrossRef](#)]
30. Li, B.; Sun, Q.; Chen, X.; Xu, Z.M.; Yang, L. Preparation and microstructure analysis of alkali-activated ground granulated blast furnace slag-steel slag grouting materials. *Case Stud. Constr. Mater.* **2024**, *20*, e03235. [[CrossRef](#)]
31. Duan, W.J.; Wu, Q.T.; Li, P.S.; Cheng, P.W. Techno-economic analysis of a novel full-chain blast furnace slag utilization system. *J. Energy* **2022**, *242*, 123049. [[CrossRef](#)]
32. Zeng, Q.; Liu, X.; Zhang, Z.; Wei, C.; Xu, C.C. Synergistic utilization of blast furnace slag with other industrial solid wastes in cement and concrete industry: Synergistic mechanisms, applications, and challenges. *J. Green Energy Resour.* **2023**, *1*, 100012. [[CrossRef](#)]
33. Zhang, Y.B.; Liu, J.C.; Su, Z.J.; Liu, B.B.; Lu, M.M.; Li, G.H.; Anderson, C.; Jiang, T. Utilizing blast furnace slags (BFS) to prepare high-temperature composite phase change materials (CPCMs). *J. Constr. Build. Mater.* **2018**, *177*, 184–191. [[CrossRef](#)]
34. Qu, A.C.; Zhao, J.; Peng, H.; Jiang, F. Recycled blast furnace slag to form-stabilize  $\text{NaNO}_3$  with high performance for high-temperature thermal energy storage. *J. Energy Storage* **2022**, *55*, 105870. [[CrossRef](#)]
35. Liu, J.; Zhang, Y.; Su, Z.; Huang, D.; Xu, D.; Lu, M.; Jiang, T. Novel low-cost anorthite porous ceramic-based binary chlorate high-temperature thermal energy storage material: Preparation and characterization. *J. Energy Fuels* **2021**, *35*, 12425–12435. [[CrossRef](#)]
36. Alibaba.com. Available online: [https://www.alibaba.com/product-detail/Buy-Best-Quality-Granulated-Blast-Furnace\\_10000008291197.html?spm=a2700.galleryofferlist.normal\\_offer.d\\_title.456726f5Epokcx](https://www.alibaba.com/product-detail/Buy-Best-Quality-Granulated-Blast-Furnace_10000008291197.html?spm=a2700.galleryofferlist.normal_offer.d_title.456726f5Epokcx) (accessed on 14 April 2024).
37. Macromicro.me. Available online: <https://sc.macromicro.me/charts/39414/global-natural-gas-prices> (accessed on 14 April 2024).
38. Wang, Y. Study on Preparation and Performance of Composite phase Change Heat Storage Material with Medium and High Temperature Stabilization. Master's Thesis, University of Chinese Academy of Sciences, Beijing, China, 2020. (In Chinese)

**Disclaimer/Publisher's Note:** The statements, opinions and data contained in all publications are solely those of the individual author(s) and contributor(s) and not of MDPI and/or the editor(s). MDPI and/or the editor(s) disclaim responsibility for any injury to people or property resulting from any ideas, methods, instructions or products referred to in the content.